ResearchGate

See discussions, stats, and author profiles for this publication at: https://www.researchgate.net/publication/272192008

A Time-Resolved Study of 1,8-Naphthalic Anhydride and 1,4,5,8-Naphthalene-Tetracarboxylic Dianhydride

ARTICLE *in* THE JOURNAL OF PHYSICAL CHEMISTRY A · FEBRUARY 2015

Impact Factor: 2.69 · DOI: 10.1021/jp511843q · Source: PubMed

READS

35

6 AUTHORS, INCLUDING:

Thiemo Gerbich

University of Wuerzburg

5 PUBLICATIONS **35** CITATIONS

SEE PROFILE

Jens Petersen

University of Wuerzburg

26 PUBLICATIONS **287** CITATIONS

SEE PROFILE

Available from: Thiemo Gerbich
Retrieved on: 26 January 2016

THE JOURNAL OF PHYSICAL CHEMISTRY A

Article

pubs.acs.org/JPCA

Time-Resolved Study of 1,8-Naphthalic Anhydride and 1,4,5,8-Naphthalene-tetracarboxylic Dianhydride

Thiemo Gerbich, Hans-Christian Schmitt, Ingo Fischer,* Jens Petersen, Julian Albert, and Roland Mitrić*

Institute of Physical and Theoretical Chemistry, University of Würzburg, Am Hubland, D-97074 Würzburg, Germany

Supporting Information

ABSTRACT: We investigate the excited electronic states of 1,8-naphthalic anhydride (NDCA) and 1,4,5,8-naphthalene-tetracarboxylic dianhydride (NTCDA) by time- and frequency-resolved electronic spectroscopy in the gas phase using picosecond lasers and by femtosecond time-resolved transient absorption in cyclohexane. The experiments are accompanied by calculations that yield the energy of the excited singlet and triplet states as well as by surface hopping dynamics simulations and calculations of spin−orbit couplings that give insight into the photochemistry. The origin of the A $^1A_1 \leftarrow X\ ^1A_1$ ($\pi\pi^*$) transition in isolated NDCA was found at 30 260 cm^{-1}, and several low-lying vibrational bands were observed. The lifetime drops sharply from 1.2 ns at the origin to around 30 ps at an excess energy of 800 cm^{-1}. Both internal conversion (IC) and intersystem crossing (ISC) are possible deactivation pathways as found in coupled electron−nuclear dynamics simulations. In cyclohexane solution, two time constants were observed. Deactivation of the initially excited state by ISC seems to dominate as supported by computations. For NTCDA we observed a gas phase lifetime of 16 ps upon excitation at 351 nm.

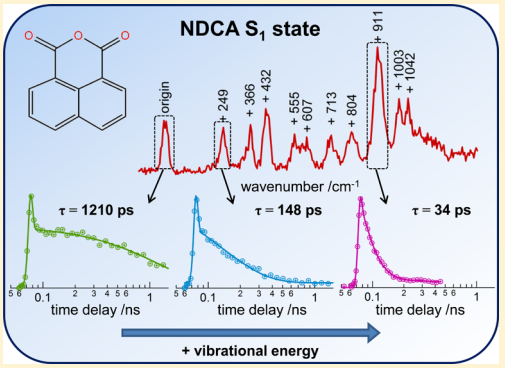

INTRODUCTION

In this work we discuss the excited state dynamics of isolated 1,8-naphthalic anhydride (NDCA) and 1,4,5,8-naphthalene-tetracarboxylic dianhydride (NTCDA) in a free jet and in solution. The experiments are supported by density functional theory (DFT) calculations that provide the energy of the excited singlet and triplet states, as well as by surface hopping simulations of the coupled electron−nuclear dynamics.

The planar NTCDA molecule, which is depicted on the right-hand side of Scheme 1, exhibits interesting optoelectronic properties. Films of it are, e.g., used in organic n-type semiconductors, thin film transistors, and organic solar cells.[1,2] This has motivated detailed investigations of the chemistry and physics of thin NTCDA films deposited on well-defined surfaces, using techniques such as X-ray absorption and photoemission spectroscopy.[3−6] Complementary to that, there is considerable interest in theory to describe the absorption and emission properties by computational methods.[7−9] Moreover, theoretical simulations are mandatory to achieve a molecular-level understanding of dynamical processes such as electronic and vibrational relaxation after photoexcitation. In this context, an important aspect that has to be addressed is the possible competition between internal conversion (IC) and intersystem crossing (ISC). Nevertheless, such computations also need to be accompanied by experiments that can provide benchmark data. For this purpose, investigations of isolated molecules are best suited since in this way any disturbing influence of the environment can be excluded. The corresponding experiments, however, are still scarce because it is difficult to generate a sufficient vapor pressure due to the high melting point of NTCDA. Only recently, the ionization energy of isolated NTCDA was measured to be 9.66 eV.[10,11] However, the high density of low-lying electronic states possibly complicates data interpretation. Therefore, we have additionally studied NDCA, depicted on the left-hand side of Scheme 1, which has a simpler structure but contains similar functionalities. Because of its lower melting point, a sufficient vapor pressure for gas phase experiments can be easily established. To gain insight into the electronic structure and dynamics of both molecules, we apply

Scheme 1. Chemical Structure of (a) NDCA (C_{2v} Point Group) and (b) NTCDA (D_{2h} Point Group)[a]

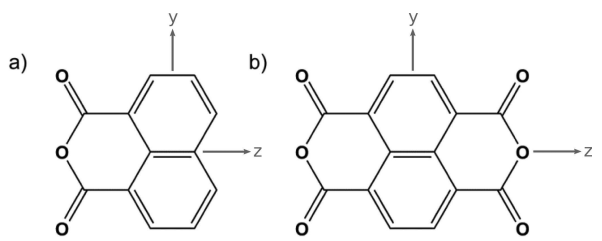

[a]The coordinate axes used for determining the symmetry are denoted in grey. The x axis lies perpendicular to the molecular plane.

Special Issue: Jean-Michel Mestdagh Festschrift

Received: November 27, 2014
Revised: February 10, 2015

ACS Publications © XXXX American Chemical Society

DOI: 10.1021/jp511843q
J. Phys. Chem. A XXXX, XXX, XXX−XXX

time- and frequency-resolved photoionization spectroscopy using a picosecond laser system. Thus, the approach in this work is similar to previous studies.[12−14] To include the competition between IC and ISC, spin−orbit coupling matrix elements between excited electronic states were explicitly calculated and incorporated in the dynamics simulations.

So far, no studies on isolated NDCA were available. Experiments in solution are also rare because the molecule hydrolyzes in aqueous environment as well as in protic solvents.[15] In a previous solution phase study a fluorescence lifetime τ_{rad} = 1.3 ns was found for NDCA in benzene.[16] Notwithstanding the lack of data for the isolated NDCA molecule, its derivatives are of considerable interest from an applicational point of view since they can be used as dyes, in liquid crystal displays, or in organic light-emitting diodes.[17−19]

EXPERIMENTAL SECTION

The molecules NDCA (m/z = 198) and NTCDA (m/z = 268) were obtained commercially from Sigma-Aldrich and were used without further purification. A melting point T_{mp} between 267 and 269 °C is given for NDCA, while T_{mp} > 300 °C for NTCDA. For the gas phase measurements the samples were thus placed in an oven attached to a pulsed solenoid valve. For NDCA, oven temperatures of 230 °C were sufficient and argon was used as carrier gas to obtain a cooled molecular beam. To reach an adequately high vapor pressure for NTCDA, the measurements were carried out in a pulsed effusive beam while heating the sample up to 260−280 °C. The molecules were expanded into a differentially pumped vacuum chamber through a 1.0 mm diameter nozzle. After a distance of 2−3 cm the pulsed free jet passed a skimmer with a diameter of 2.0 mm and entered the experimental chamber with a pressure of 5.0−8.5 × 10^{-7} mbar. The detailed setup of the apparatus has been described in a previous publication.[20]

In the experimental chamber the molecules were ionized by a picosecond laser (Ekspla) with a repetition rate of 10 Hz. A solid state Nd:YLF (neodymium-doped yttrium lithium fluoride) laser with a wavelength of 1053 nm and a pulse width of 8 ps is the central part of the system. The main part of the 351 nm third harmonic (7−8 mJ) was employed to pump an optical parametric generator (OPG) to generate tunable pump pulses, while a small amount (200−300 μJ) was split off and sent over a motorized linear translation stage to be used as the probe pulse. Note that for time-resolved experiments on NTCDA the 351 nm third harmonic was the pump and the OPG output the probe pulse. The OPG output between 280 and 350 nm yielded pulses with a bandwidth of approximately 20 cm^{-1} and a pulse energy of 30 to 100 μJ. The instrument response function (IRF) was determined to be around 5 ps. The pump and probe pulses were overlapped in front of the experimental chamber using a dichroic mirror. For NDCA, unfocused pulses yielded the best signal-to-noise ratio (SNR), while the NTCDA measurements required slightly focused OPG pulses to achieve a sufficient ion signal. Ions were accelerated in a mass spectrometer onto a multichannel plate (MCP) detector. The data were averaged for 100 shots per point for every scan; and six to 12 scans were averaged to receive a good SNR.

For the transient absorption (TA) spectra in solution a Solstice/Topas-C (Newport/Spectra Physics) laser system with a repetition rate of 1 kHz was employed. The NDCA samples were dissolved in high-purity cyclohexane (Sigma-Aldrich, ChromasolvPlus), and the solution was purged with argon for 15 min. For the measurements a 2 mm quartz cuvette equipped with a microstirrer was used. The TA-signal was recorded in a Helios TA spectrometer. The pump pulses (338, 321, and 310 nm) with pulse energies of 300 nJ were generated in an OPG (Light Conversion Topas-C), while the white light probe pulses were generated in a moving CaF_2 crystal. The resulting IRF of the system was found to be approximately 140 fs. A more detailed description of the setup has been reported elsewhere.[21] For evaluation of the recorded TA-maps the data was deconvoluted by a global fitting routine using the program Glotaran.[22]

COMPUTATIONAL SECTION

The structures of NDCA and NTCDA have been optimized in the framework of density functional theory (DFT) employing the CAM-B3LYP functional[23] combined with the def2-TZVP basis set,[24] and the energy minima have been confirmed by calculating the vibrational frequencies. Subsequently, the vertical electronic absorption spectra of NDCA and NTCDA have been calculated using time-dependent density functional theory (TDDFT) employing the same functional and basis set as stated above. In order to determine the vibronic transitions between the electronic ground state and the two lowest electronically excited states of NDCA, the structures have been also optimized in the excited states, the vibrational frequencies have been determined, and finally the vibrationally resolved absorption spectrum has been calculated following the method of Santoro et al.[25,26] Solvent effects for several spectra have been accounted for using the polarizable continuum model (PCM).[27] All DFT calculations have been performed using the Gaussian 09 program package.[28]

The coupling between singlet and triplet states has been investigated by calculating spin−orbit matrix elements between the singlet and triplet manifolds for selected DFT-optimized geometries of NDCA. The spin−orbit coupling has been calculated using the Molpro program package,[29,30] employing the multireference configuration interaction method (MR-CI)[31−33] with reference configurations taken from a complete active space self-consistent field (CASSCF)[34,35] calculation. For this purpose, the 6-31G basis set[36] has been employed, and the active space consisted of 8 electrons in 5 orbitals, while for the MRCI all single and double excitations from the active orbitals to higher virtual orbitals were taken into account.

The nonradiative relaxation from the first electronically excited singlet state to the ground state has been investigated employing Tully's surface hopping method.[37] For this purpose, initial coordinates and momenta were sampled from a 20 ps long trajectory using the semiempirical OM3 method.[38] The nonadiabatic dynamics was then performed using the OM3 method combined with MR-CI[39,40] in the framework of the MNDO program,[41] and all single and double excitations out of the ground state SCF and the HOMO−LUMO excited configuration were taken into account. The nuclear trajectories were propagated numerically by solving Newton's equations of motion using the velocity Verlet algorithm[42] with a time step of 0.2 fs. The electronic state coefficients needed for determining the hopping probabilities between electronic states have been calculated along each trajectory by numerical integration of the time-dependent Schrödinger equation including the non-adiabatic coupling.

Similarly, also nonadiabatic dynamics simulations within the four lowest triplet states were performed over ∼100 fs in order

DOI: 10.1021/jp511843q
J. Phys. Chem. A XXXX, XXX, XXX−XXX

to obtain average values for the nonadiabatic coupling elements in the triplet manifold (see below).

In addition to the nonadiabatic dynamics in the singlet states, the electronic state population dynamics in the full manifold of two singlet and four triplet states has been simulated on a model level. For this purpose, the energies and spin−orbit couplings have been initially assigned the values obtained for the S_1 or S_0 state minimum structures, respectively. The nonadiabatic couplings have been averaged from surface-hopping simulations in the singlet and triplet manifolds as described above, and the time-dependent Schrödinger equation

$$i\hbar\dot{c}_i = E_i c_i - \sum_j (i\hbar D_{ij} - H_{ij}^{SO}) c_j \quad (1)$$

including the electronic energies E_i, the nonadiabatic couplings D_{ij}, and the spin−orbit couplings H_{ij}^{SO} has been solved numerically over a time duration of 50 ps. In order to mimic the fluctuations of energies and couplings due to nuclear motion, the initial values have been modified in each step by a random term, which for the energies did not exceed 0.05 eV, while for the couplings a variation of the same size as the initial coupling was enabled.

RESULTS

The excitation energies and symmetry labels of the lowest singlet and triplet states of the two molecules are summarized in Table 1, and the energetic ordering is illustrated in Figure 1.

Table 1. Vertical Excitation Energies of the Low-Lying Electronic States of Isolated NDCA and NTCDA at the S_0 Minimum Geometry, Determined by TDDFT Calculations[a]

NDCA			
singlet states (eV)		triplet states (eV)	
$^1A_1$	4.17 (3.60)	$^3A_1$	2.32 (1.62)
$^1B_2$	4.40 (4.22)	$^3B_2$	3.55 (3.26)
$^1B_1$	4.63 (4.36)	$^3B_2$	3.83 (3.55)
		$^3B_1$	4.21 (3.99)
NTCDA			
singlet states (eV)		triplet states (eV)	
$^1B_{1u}$	3.84	$^3B_{1u}$	2.03
$^1B_{2u}$	4.12	$^3B_{2u}$	3.27
$^1B_{2g}$	4.27	$^3B_{3g}$	3.43
$^1B_{3u}$	4.40	$^3B_{2g}$	3.89
		$^3B_{3u}$	3.99

[a]For NDCA, also the values obtained at the S_1 minimum geometry are given in parentheses. The symmetry assignment corresponds to the coordinate system indicated in Scheme 1.

In addition, the corresponding absorption spectra derived from computed vertical excitation energies and oscillator strengths are shown in Figure 2.

As visible, several excited states are accessible upon near-UV excitation. The lowest vertical excitation energies were determined to be 4.17 eV (297.3 nm) for NDCA and 3.84 eV (323.1 nm) for NTCDA. Since NDCA is of C_{2v} symmetry, transitions into the A $^1A_1$, B $^1B_2$, and C $^1B_1$ states are dipole-allowed. The A $^1A_1$ ← X $^1A_1$ transition has $\pi^* \leftarrow \pi$ character, and consequently, a high oscillator strength of f_e = 0.20 has been computed.

For NTCDA, which is of D_{2h} symmetry, a $^1B_{1u}$ ($\pi\pi^*$) state was computed to be the first excited singlet state. Again, a high oscillator strength of f_e = 0.31 has been found. The vertical excitation energies differ significantly (on the order of 0.5 eV) from those reported for selected transitions in recent work.[43] As visible in Figure 1 both molecules possess numerous low-lying triplet states. Since $n\pi^*$ triplet states with only a small energy gap $\Delta E_{S_1T_n}$ exist, efficient intersystem crossing (ISC) is allowed in both molecules according to the El-Sayed rules,[44] as highlighted by green arrows in Figure 1. In contrast, El-Sayed-forbidden ISC transitions are marked in red. On the basis of the computed excited state energies for both NDCA and NTCDA, an excited state deactivation via internal conversion (IC) or ISC should be possible.

1. Gas Phase Studies on NDCA. The ionization energy (IE) of NDCA in the gas phase was determined to be 8.98 eV by photoelectron spectroscopy.[11] No experimental data are available on the excited states of isolated NDCA, but UV/vis spectra in a number of different solvents yielded the first absorption bands between 338 and 350 nm.[16] Thus, after excitation of the NDCA S_1 state a two-photon ionization step is required for ionization. The [1 + 2′] resonance-enhanced multiphoton ionization (REMPI-) spectrum of NDCA is depicted in Figure 3. It was obtained upon tuning the OPG output and using the 351 nm third harmonic for ionization around the zero in time. The first band appears at 30 260 cm^{-1} (330.5 nm) and is assigned as the origin of the A $^1A_1$ ← X $^1A_1$ transition. No additional transition has been found upon scanning 1250 cm^{-1} further to the red. To higher energies, a number of distinct vibronic bands are observed.

For excitation wavenumbers above approximately 31 000 cm^{-1} a broad background signal increases, but structure is still visible. The assignment of the first band at 30 260 cm^{-1} (3.752 eV) to the origin of the A ← X transition is in excellent agreement with TDDFT-calculations predicting an excitation energy of 3.777 eV for the A (S_1) (v' = 0) ← X (S_0) (v'' = 0) transition. Note that the experimental value is accurate to within ±10 cm^{-1}, due to the bandwidth of the picosecond laser. Moreover, since the lowest vibronic excitation energy to the second excited electronic state has been calculated at 4.200 eV (33 870 cm^{-1}), it can be ascertained that the observed vibrational structure entirely stems from vibronic transitions into the first excited state. Most of the vibronic bands visible in the spectrum can be assigned to totally symmetric in-plane bending modes of the NDCA ring system, often with considerable ring breathing character. In some cases several transitions with similar wavenumbers are possible carriers. An exception is the comparably intense band at +249 cm^{-1}, because no totally symmetric band was computed in this wavenumber region. Possible assignments are an overtone of a b_1 out-of-plane mode or a b_2 fundamental. For the former assignment, the relatively large intensity is unusual, while the second would require vibronic coupling with a B_2 electronic state, for example, the S_2 state. However, since according to the computations the +249 cm^{-1} band is energetically well separated from the origin of the S_2 ← S_0 vibronic manifold, such a coupling is also expected to be small. The relative positions of the observed bands and a comparison to vibronic transitions calculated to lie nearby are given in Table 2.

In the next step we investigated the excited state dynamics by [1 + 2′] ps-time-resolved photoionization, again using the 351 nm third harmonic of the Nd:YLF laser for the two-photon

DOI: 10.1021/jp511843q
J. Phys. Chem. A XXXX, XXX, XXX−XXX

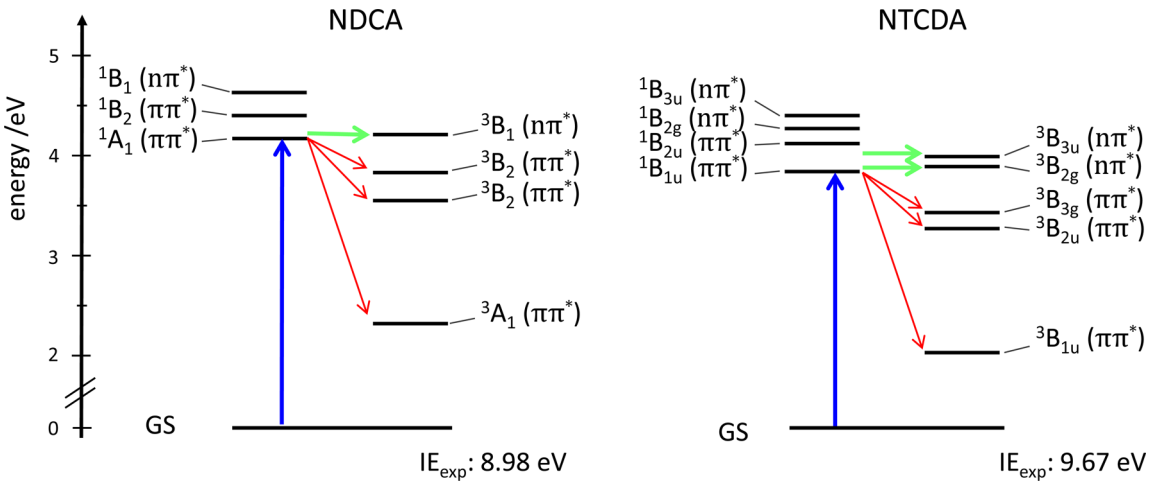

Figure 1. Electronic states of NDCA and NTCDA determined by TDDFT calculations. The green arrows highlight El-Sayed-allowed ISC deactivation pathways, while transitions marked in red are El-Sayed-forbidden.

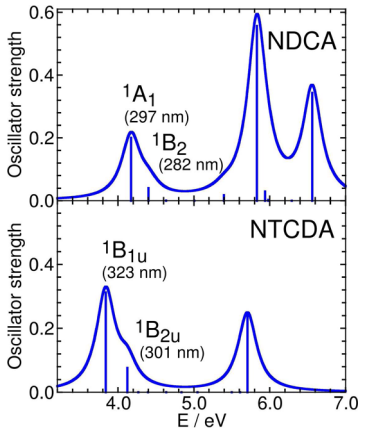

Figure 2. Calculated vertical electronic absorption spectra of NDCA and NTCDA obtained using TDDFT with the CAM-B3LYP functional and def2-TZVP basis set. The spectra have been broadened by a Lorentzian with a width of 0.3 eV.

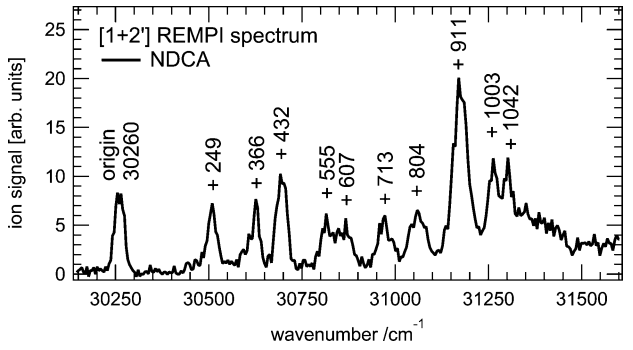

Figure 3. [1 + 2′] REMPI spectrum of isolated NDCA at the time zero, corrresponding to the $S_1 \leftarrow S_0$ transition. For ionization a 351 nm pulse was employed. The peak at 30 260 cm^{-1} is assigned to be the band origin.

ionization step. The first ten vibronic bands, all visible in Figure 3, and in addition a higher band at +2222 cm^{-1} were excited and their lifetimes τ were probed. In Figure 4 four selected decay-traces at different excitation wavelengths are shown. The decay was fitted by a single exponential function. In addition a contribution described by the instrument function was present around t_0, possibly due to higher order processes. For the S_1 origin a lifetime in the nanosecond (ns-) regime was found (top trace of Figure 4). However, τ decreases quickly upon excitation and reaches values of some 10 ps for higher S_1 vibronic states.

At higher excitation energies an offset is visible at long delay times. The signal rises within 5 ps, given by the IRF. It is remarkable that for the origin of the S_1 state the lifetime is found to be in the ns-regime (1.21 ns), while for the next transition (+ 249 cm^{-1}) it drops sharply to nearly a tenth of this value (134 ps). Within the next few vibronic bands a further decrease of the time constant is observed, until the lifetimes reach an almost constant value of 27 to 30 ps for the higher vibronic bands. Figure 5 depicts the time constants on a logarithmic scale compared with the REMPI spectrum.

In addition to the NDCA monomer signal at m/z = 198 two smaller peaks appeared in the photoionization mass spectrum (cf. Figure S1). These signals at m/z = 154 and m/z = 126 are fragments of NDCA due to loss of CO_2 and CO_2 + CO, respectively. The peaks show the same time dependence as the parent ion and thus originate from dissociative photoionization.

2. Transient Absorption Studies on NDCA. We additionally investigated the NDCA photophysics in cyclohexane (CH) by transient absorption (TA) spectroscopy. For nonpolar solvents only a small shift of the excited state energies compared to the isolated molecule, and a similar dynamics are expected. Such studies therefore aid in assigning the deactivation pathways in NDCA. In the UV/vis absorption spectrum three bands appear with maxima at 338, 321, and 310 nm due to vibronic structure (cf. Figure S2). Therefore, the S_1 origin in CH is slightly shifted to the red. At each of the three bands, TA measurements were conducted and similar dynamics was found.

In Figure 6 the transient spectra of NDCA recorded at an excitation wavelength of 321 nm are plotted at selected time delays to illustrate the evolution of the TA signal. The black line in Figure 6 represents a spectrum where the white light probe pulse arrived before the excitation pulse. Immediately after excitation a broad band at 492 nm appears together with a smaller band at 385 nm (red line). Over a period of several hundred ps, the signal decreases and the maximum shifts to the blue. After roughly 200 ps the band maximum has moved to 470 nm, from thereon the change in signal is small and the

DOI: 10.1021/jp511843q
J. Phys. Chem. A XXXX, XXX, XXX−XXX

Table 2. Positions of Vibronic Bands in the REMPI-Spectrum of Isolated NDCA Compared to Calculated Vibronic Transitions from the Lowest Vibrational State of S_0 into the S_1 State

exc. wavelength (nm)	rel. position (cm^{-1})	computed vibronic transition (cm^{-1})	possible S_1 vibrational state	gas phase lifetime (ps)
330.5	0 (origin)	328.4 nm (origin)	0−0 transition	1.21×10^3
327.7	+249	+274/+285	$(10\ b_1)^2/19\ b_2$	134
326.5	+366	+361	20 a_1	50
325.8	+432	+440/+454	19 a_1/18 a_1	47
324.5	+555	+580	17 a_1	43
323.9	+607	+667[a]	16 a_1[a]	37
322.8	+713	+667[a]	16 a_1[a]	35
321.9	+804	+822	15 a_1	27
320.8	+911	+961/+908/+894	14 a_1/$(18\ a_1)^2/(18\ a_1)^1(19\ a_1)^1$	29
319.8	+1003			30
307.9	+2222			22

[a]In the computations the 16 a_1 appears with significant intensity, but lies in between the bands at 607 and 713 cm^{-1}.

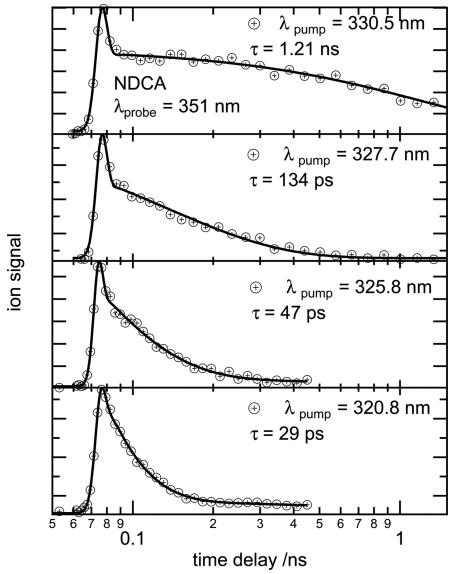

Figure 4. Selected time-delay traces of isolated NDCA. The pump wavelengths are indicated in the figure, for the probe a wavelength of 351 nm was employed. While for the origin band at 330.5 nm (top trace) a ns-time constant was found, for slightly higher excitation energies the lifetimes dropped sharply, eventually reaching a constant level of roughly 20−30 ps (bottom trace). In the two lower traces a small offset is visible at long time delays.

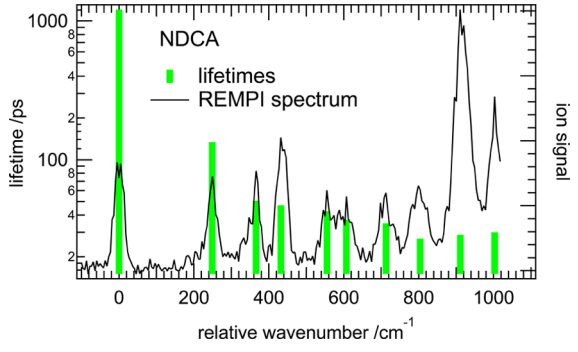

Figure 5. Summary of the lifetimes measured for the various vibronic state of NDCA (green columns). The low-energy part of the MPI-spectrum is also shown in the graph (solid line).

band has considerable intensity even after 7.5 ns. The smaller band centered at 385 nm disappears on the order of several

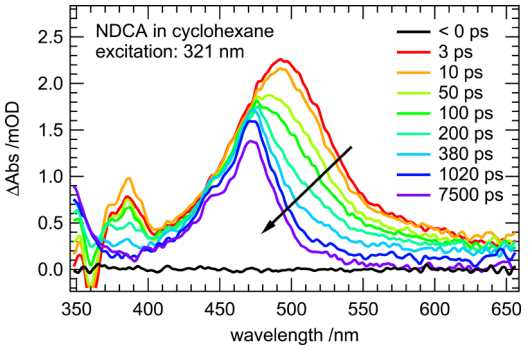

Figure 6. Transient absorption spectra of NDCA in cyclohexane for selected time delays recorded at 321 nm excitation.

hundred ps. Simultaneously with the decrease of the 492 nm band, the edge of a band at 350 nm grows in, which is not visible at short delay times.

From a global fit to the spectra two time constants can be extracted. For the short time process, associated with the blue shift of the major band and the disappearance of the 385 nm band, a time constant τ_1 of τ_1 = 193 ps was extracted. In addition there is a long-lived contribution. The time constant τ_2 of this long-living state can only be estimated to be at least 30 ns or more. These data hint at a two-step process, deactivation of the photoexcited state with a time constant τ_1 and subsequent formation of a long-lived state. The global fits of the TA spectra recorded at 338 and 310 nm yielded similar dynamics and are not further discussed. From the appearance of the absorption band around 470 nm, which is not present in the static absorption spectrum of NDCA, it can be inferred that the molecule has not returned to the singlet ground state on the nanosecond time scale. A comparison with a calculated absorption spectrum of the T_1 triplet state as depicted in Figure 7 shows full agreement with the experimental data. Thus, we can assign the observed decay constant τ_1 in cyclohexane to an ISC process.

3. Nonadiabatic Dynamics Simulations and Spin−Orbit Coupling. To gain additional molecular-level information on the interplay of different dynamical processes in photoexcited NDCA, further theoretical investigations have been performed. First, in order to determine the time scales of internal conversion (IC) within the singlet manifold, surface-hopping molecular dynamics simulations have been carried out as described in the Computational Section. For NDCA in the gas phase, IC from the first excited to the ground electronic

DOI: 10.1021/jp511843q
J. Phys. Chem. A XXXX, XXX, XXX−XXX

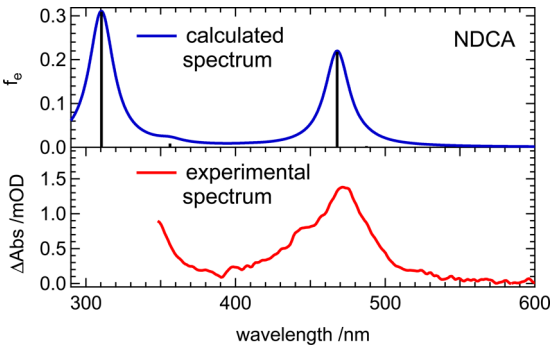

Figure 7. Comparison of the computed triplet absorption spectrum of NDCA obtained using TDDFT (CAM-B3LYP, def2-TZVP basis set, and PCM for solvent cyclohexane) with the experimental transient absorption spectrum measured 7.5 ns after initial excitation (cf. Figure 6).

state has been found to occur with a strongly temperature-dependent rate. For a low temperature of 30 K, corresponding to the conditions approximately present in the gas phase experiments, depopulation of the first excited singlet state is slow on the time scale of the simulation, with a ground state population of ∼10% after 20 ps, while for higher temperatures this value increases significantly (cf. Figure S4). The relaxation mechanism involves a conical intersection between the S_1 and S_0 states, through which efficient population transfer can take place.

Besides the dynamic processes involving singlet states only, also ISC processes and subsequent relaxation within the triplet manifold may be significant. Therefore, we calculated the spin−orbit coupling matrix elements between the singlet S_0 and S_1 and the four lowest-lying triplet states for selected nuclear geometries of NDCA, as presented in Table 3. As already

Table 3. Spin−Orbit Coupling Matrix Elements of NDCA for the DFT-Optimized Geometries of the S_0 and S_1 States; the Absolute Values in cm^{-1} Are Given

state	S_0 ($^1A_1$)		S_1 ($^1A_1$ $\pi\pi^*$)	
opt. geometry	S_0	S_1	S_0	S_1
T_1 ($^3A_1$ $\pi\pi^*$)	0.0	0.0	0.0	0.0
T_2 ($^3B_2$ $\pi\pi^*$)	2.9×10^{-2}	2.5×10^{-2}	6.4×10^{-2}	3.9×10^{-2}
T_3 ($^3B_2$ $\pi\pi^*$)	4×10^{-3}	5×10^{-3}	5.4×10^{-2}	7.2×10^{-2}
T_4 ($^3B_1$ $n\pi^*$)	45.9	42.7	10.3	11.8

alluded to above, in particular the spin−orbit couplings between $n\pi^*$ and $\pi\pi^*$ states can become quite substantial in organic molecules. In fact, we computed values around 10 cm^{-1} for the coupling between the $\pi\pi^*$ S_1 and the close-lying $n\pi^*$ T_4 state and about 45 cm^{-1} between S_0 and T_4, while between all pairs of $\pi\pi^*$ states the coupling is almost negligible.

The size of the spin−orbit couplings should be compared to that of the nonadiabatic couplings for the competing IC processes. For the relaxation from S_1 to S_0, our surface-hopping simulations provided average dynamical couplings on the order of 4 cm^{-1} at 30 K up to 9 cm^{-1} at 300 K. However, in all cases, close to conical intersections the nonadiabatic coupling sharply rises, up to values of typically 1000−5000 cm^{-1}. Therefore, the observed decrease in the excited state lifetime with increased temperature/internal vibrational energy can be mainly attributed to a faster approach to the conical intersections, where the nonadiabatic coupling is large and electronic transitions occur, while the average couplings for nuclear arrangements remote from these points are only slightly changed. These latter couplings are of the same order of magnitude as the spin−orbit couplings for the El-Sayed-allowed ISC transition T_4 ($n\pi^*$) ← S_1($\pi\pi^*$), which represents the competing pathway to the S_0 ← S_1 IC process. However, far away from S_1/S_0 conical intersections, the energy gap between S_1 and T_4 is much smaller than that between S_1 and S_0 (in fact, S_1 and T_4 may even become near-degenerate); according to the energy gap law, ISC transitions may thus be more efficient than IC in the singlet manifold, at least unless an S_1/S_0 conical intersection is reached.

This reasoning can be further supported by model calculations of the electronic state population dynamics. For this purpose, we selected the two lowest singlet and the four lowest triplet states and numerically solved the time-dependent Schrödinger eq 1 in this manifold, including nonadiabatic and spin−orbit couplings, as described in the computational section. To account for the relaxation of the molecule in the S_1 state after initial excitation, the numerical values for the electronic energies obtained at the minimum energy structure in the S_1 state, as given in parentheses in Table 1, were used. In addition, the spin−orbit couplings from Table 3 and the averaged nonadiabatic couplings between S_1 and S_0 as well as between the triplet states as obtained from surface-hopping dynamics were employed. The numerical values are provided in Table 4.

Table 4. Average Nonadiabatic Coupling Matrix Elements of NDCA Obtained from Surface-Hopping Dynamics Simulations in the Singlet and Triplet Manifolds, Respectively

pair of states	coupling (cm^{-1})
S_0/S_1	9
$T_1/T_{2,3,4}$	22
T_2/T_3	650
T_2/T_4	220
T_3/T_4	650

In order to account for effects of nuclear dynamics on energies and couplings, we allowed these quantities to vary stochastically about their initial values, in this way mimicking the fluctuations caused by nuclear motion in a very simplified way. The resulting temporal behavior of energies and couplings is illustrated in Figure 8a,b. Notice that without these variations, the couplings would be constant, thus only leading to Rabi-type oscillations of the electronic state coefficients without residual population transfer.

Our simulations showed that on a time scale of approximately 50 ps, almost 20% of the population is transferred from the initially populated S_1 to the triplet manifold via the $n\pi^*$-type T_4 state, as shown in Figure 8c. If, instead, the model is constructed using the energies and couplings obtained for the S_0 geometry, which implies a reduction of the S_1/T_4 energy gap from 0.4 eV to about 0.04 eV (cf. Table 1 for energies and Table 3 for spin−orbit couplings), the population transfer is, according to the energy gap law, even more pronounced and reaches more than 20% within 50 ps (cf. Figure S5, Supporting Information). The S_0 population remains negligible in both cases. This means that, if no conical intersection of S_1 with the ground state is reached, triplet state

DOI: 10.1021/jp511843q
J. Phys. Chem. A XXXX, XXX, XXX−XXX

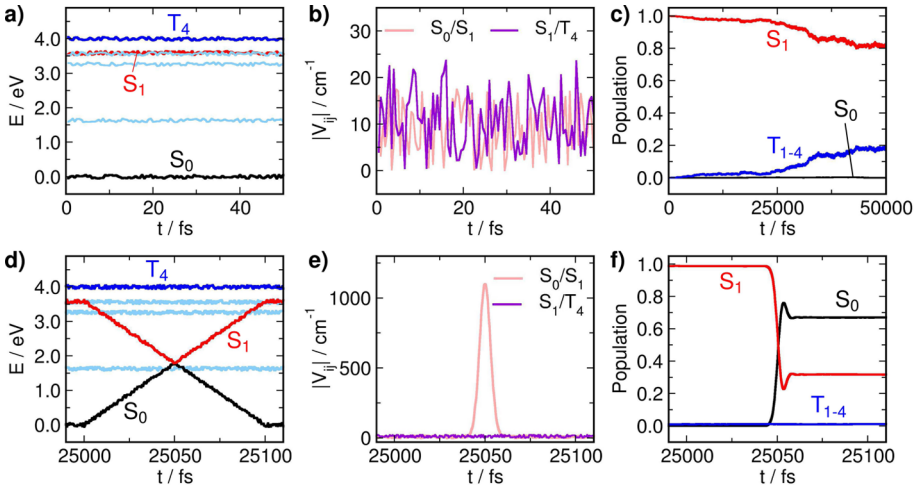

Figure 8. Model calculations of electronic relaxation dynamics in NDCA involving singlet and triplet states. Upper panels: (a) Electronic energies of the S_0 (black) and S_1 states (red), and the triplet states T_4 (blue) and T_1−T_3 (light blue). (b) Nonadiabatic coupling between S_0 and S_1 (light red), as well as spin−orbit coupling between S_1 and T_4 (violet). The energies and couplings are modeled to randomly fluctuate around the values obtained at the S_1 state minimum geometry and behave in the entire simulation similarly to the time period presented here. (c) Resulting population dynamics obtained for a simulation time of 50 ps. Lower panels (d−f): Results of a model calculation similar to the upper panels, but including the effect of a conical intersection between S_0 and S_1. For this purpose, around an arbitrarily selected time t = 25 000 fs, an electronic degeneracy as well as an increased S_0/S_1 nonadiabatic coupling are introduced. The degeneracy is constructed by closing and restoring the energy gap $\Delta E = E_{S_1} - E_{S_0}$ as a linear function of time within 100 fs (cf. panel d). The nonadiabatic coupling is modeled by a Gaussian function as $D_{S_1/S_0} = D_{max} \exp(-(4 \ln 2/w^2)\Delta E^2)$, with w = 0.51 eV and D_{max} = 1097 cm^{-1}.

populations up to 20% may be obtained within the simulation time of 50 ps.

The effect of conical intersections can also be added to the model. For this purpose, the S_1/S_0 energy gap is gradually closed during the simulation (cf. Figure 8d), and at the same time the nonadiabatic S_1/S_0 coupling is increased up to a value of approximately 1000 cm^{-1} when the energetic degeneracy of the two states is reached, as shown in Figure 8e. Subsequently, the energy gap is increased again, and the nonadiabatic coupling is reduced back to the average value determined for configurations away from conical intersections. For such a case, the simulations show pronounced population transfer to the S_0 state up to 70% (cf. Figure 8f).

These model calculations show that both IC and ISC may be the dominant relaxation processes, depending on whether a conical intersection between the singlet states S_1 and S_0 is reached or not. From the full coupled electron−nuclear nonadiabatic dynamics simulations in the singlet manifold described at the beginning of this section, the height of the energy barrier that needs to be overcome in the S_1 state in order to reach a conical intersection can be estimated to about 0.7−0.9 eV. The kinetic energy of trajectories thermalized at 30 K amounts to about 0.07 eV and is thus on average too low to get over the barrier, hence the long lifetime in the excited state. At 300 K, by contrast, the average kinetic energy is about 0.74 eV, and thus, the barrier can be overcome (cf. also Figure S4).

4. Gas Phase Studies of NTCDA. The NTCDA time-of-flight mass spectrum was observed in a one-color REMPI measurement with focused picosecond laser pulses, cf. Figure S1. For the ionization energy of isolated NTCDA, values of 9.67[11] and 9.66 eV[10] have been reported. Thus, similar to NDCA, the photoionization of isolated NTCDA requires three photons in the 260−385 nm region. In the time-of-flight mass spectrum of NTCDA (m/z = 268) a characteristic fragment appears at m/z = 224, corresponding to loss of a CO_2 unit by dissociative photoionization.[8] Photoionization mass spectra using 118 nm radiation (Nd:YAG ninth harmonic produced in Xe) yielded the same mass spectrum with similar intensities.

Figure 9 shows the one-color [1 + 2] REMPI spectrum of NTCDA recorded between 290 and 345 nm with the

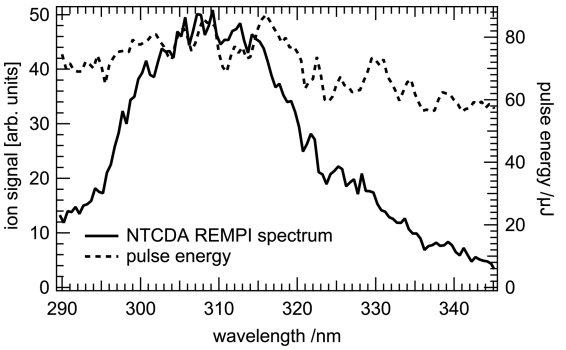

Figure 9. One-color REMPI spectrum of NTCDA as well as the corresponding pulse energy of the excitation wavelengths.

picosecond-laser system. On the basis of the computations shown in Figure 1, this corresponds to excitation into one of the two lowest-lying singlet states (S_1 or S_2). Starting from 345 nm the signal increases quickly and reaches a maximum at 309 nm. The band is broad and unstructured. Beyond 345 nm the pulse energy of the OPG drops sharply but is fairly constant over the depicted energy range. We were not able to record a decay trace in this wavelength region. In agreement with the broad spectrum we assume that the dynamics of NTCDA in this wavelength region is dominated by an ultrafast deactivation process with a subpicosecond time constant.

The computed vertical excitation energy to the A $^1B_{1u}$ (S_1) state is 3.84 eV (323.1 nm). Since the transition between the vibrational ground states of the two electronic states will be somewhat lower in energy (cf. the red-shift of ∼0.4 eV in the

DOI: 10.1021/jp511843q
J. Phys. Chem. A XXXX, XXX, XXX−XXX

case of NDCA), we employed the 351 nm (3.53 eV) third harmonic of the Nd:YLF laser for excitation to pump the S_1 state. In the next step we recorded a time-delay trace by ps-time-resolved [1 + 2′] photoionization. For ionization, the OPG output at 326.5 nm was slightly focused to obtain a good signal/noise ratio. In Figure 10 the resulting delay scan of

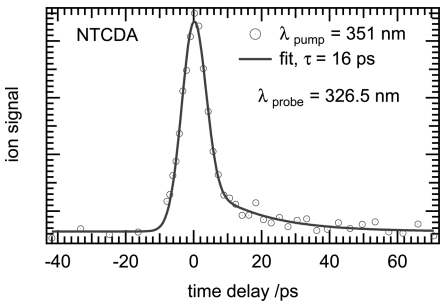

Figure 10. Time-delay trace of isolated NTCDA at an excitation wavelength of 351 nm. A monoexponential decay of 16 ps was found.

NTCDA is depicted. The data points were fitted with a monoexponential function, which was convoluted with the IRF. Twelve separate scans were averaged and yielded a time constant of 16 ps. To exclude that the dynamics is caused by a two-photon excitation to a higher electronic state we varied the pulse power of the pump pulse at the zero in time and observed a linear dependence of the signal on the laser power. Accordingly the time constant of 16 ps is assigned to the deactivation process of the NTCDA S_1 state.

DISCUSSION

The results shown in the preceding sections provide considerable information on the nonradiative processes in NDCA. Two competing deactivation pathways are possible for the S_1 state of both molecules, internal conversion (IC) to the electronic ground state and intersystem crossing (ISC) to a triplet state. The calculations of the nonadiabatic relaxation within the singlet manifold reveal a possible deactivation to the ground state via a conical intersection. This process is computed to take place on a time scale of several tens of picoseconds, with a strong dependence on the temperature/internal vibrational energy of the molecule. Although the computed time scales are systematically lower than the experimentally obtained decay rates presented in Table 2, they show a qualitatively similar decrease with increasing internal vibrational energy. However, as indicated in Figure 1, also several triplets lie close to or below the first excited singlet state S_1. In particular, the energy gap between the S_1 and the $n\pi^*$-type triplet state T_4 only amounts to 0.04 eV. According to the energy gap law for radiationless transitions,[45,4647] this should favor ISC transitions according to

$$k_{ISC} = k_0\, e^{-\Delta E/kT} \qquad (2)$$

Moreover, the computations described above indicate that considerable spin−orbit coupling is present between singlet and triplet states of $\pi\pi^*$ and $n\pi^*$ character, respectively, according to the El-Sayed rules.[44] The corresponding transition T_4 ($n\pi^*$) ← S_1 ($\pi\pi^*$) is indicated in Figure 1 by a green arrow. Taking into account the same order of magnitude of the spin−orbit couplings and the average nonadiabatic couplings between S_1 and S_0 for geometries far off conical intersections (cf. Section 3), it is likely that ISC can compete with IC unless a S_1/S_0 conical intersection is reached, thus enabling population transfer to the triplet manifold.

Deactivation by ISC is supported by the solution phase data, which reveal a long-lived state with an absorption spectrum that can be assigned to the triplet state based on the computations, as discussed above. Most likely, ISC in solution proceeds via the El-Sayed allowed T_4 ($n\pi^*$) ← S_1 ($\pi\pi^*$) pathway within roughly 200 ps. The T_4 state subsequently deactivates quickly to the T_1 state with a time constant that is too fast to be observed in our experiments. Time constant τ_2 then represents the lifetime of the T_1 state. Note that phosphorescence in NDCA solutions has been reported before with μs-lifetimes,[48] and the TA spectrum after 7.5 ns looks similar to the phosphorescence bands in methanol,[48] supporting this interpretation. The offset observed in the gas phase experiments might correspond to this long-lived triplet state as well. The 200 ps time constant τ_1 agrees well with the lifetimes of low-lying vibronic states in the gas phase spectrum. It should be kept in mind that vibrationally excited states in solution cool quickly by energy transfer to solvent molecules,[47] thus a comparison to the low-lying states of the isolated molecule is adequate.

However, while for the solution phase deactivation via ISC appears to be evident from the measured transient absorption spectra, the situation is less clear for the gas phase experiments. The rate constants τ_1 obtained in the experiment might well be due to both IC and ISC processes. Although at first glance the time constants seem to be rather short for ISC, there have been reports on fast ISC for numerous carbonyl compounds. In benzophenone, for example, a time constant τ_{ISC} of 5 ps was found for T_2 ($\pi\pi^*$) ← S_1 ($n\pi^*$).[49] For 1-nitronaphthalene, the molecule with the fastest known S_1 deactivation by ISC, τ_{ISC} was determined to be less than 100 fs.[50] In the enol form of isolated cytosine, IC and ISC were found in a computational analysis to compete in the S_1 deactivation with lifetimes of a few ps,[51] and the computed spin−orbit couplings assumed a comparable magnitude as in the calculations presented here. Thus, a deactivation by ISC on the 10−100 ps scale is not unusual.

In principle, molecules both in the excited singlet as well as in the triplet states can be ionized by the applied ionization scheme: The use of two photons of 351 nm yields an energy of about 7.1 eV, while the computed adiabatic ionization energy from the T_1 state to the cation ground amounts to 6.4 eV. For the S_1 state, a value of only 5.0 eV is obtained. Although both pathways are present, the determination of a branching ratio requires, e.g., photoelectron spectroscopy as a probe method. A setup to conduct such experiments is currently under construction.

Interestingly, for excitation at the S_1 origin of the isolated molecule, a much longer lifetime of 1.2 ns was found. The fast decrease of τ_1 with vibrational excitation points at a competition of deactivation channels around the S_1 origin that depends sensitively on the energy. The computations show a deactivation time that decreases strongly with temperature, possibly because of a barrier along the way to the crossing point. At higher temperatures there is enough internal energy in the molecule to overcome this barrier, while excitation to the S_1 origin does not seem to provide enough energy to overcome the barrier. Thus, the approach to the conical intersections is hindered, coupling to the ground state remains weak, and deactivation by IC is slow. Once additional vibrational excitation is placed in the molecule, the crossing point can be accessed and return to the ground state proceeds much faster.

DOI: 10.1021/jp511843q
J. Phys. Chem. A XXXX, XXX, XXX−XXX

However, because of the presence of large spin−orbit coupling between $n\pi^*$ and $\pi\pi^*$ states already at the initial stage of the dynamics, part of the excited state population undergoes ISC to the triplet manifold. There the population resides on a much longer time scale, giving rise to the observed long-time offset in the gas phase time-delay traces. However, in cyclohexane solution τ_1 is always on the 100−200 ps scale. Although the influence of cyclohexane on molecular potential energy surfaces is generally small, it enables efficient dissipation of vibrational energy, such that a strong dependence of the relaxation time constants on the initial vibrational excitation is not observed. Moreover, this thermalization seems to sufficiently slow down the approach to conical intersections between the S_0 and S_1 states such that ISC to the triplet manifold becomes a major deactivation channel. This eventually leads to observation of the triplet absorption for delay times up to several ns (cf. Figures 6 and 7).

For NTCDA a similar situation is evident. Several triplet states lie close to the S_1 and a small energy gap is predicted by the computations for the photoexcited $S_1(\pi\pi^*)$ and the triplet states of $n\pi^*$ character, T_3 and T_4. Hence a competition of deactivation pathways via ISC and IC is likely for isolated NTCDA as well.

CONCLUSION

The dynamics of the S_1 state of NDCA has been investigated by both theory and experiment. The origin of the $A\ ^1A_1 \leftarrow X\ ^1A_1$ ($\pi\pi^*$) transition is found at 30 260 cm^{-1} (3.752 eV), in very good agreement with the computational value of 3.777 eV. Several low-lying vibronic bands were observed that could be assigned to in-plane bending modes based on the computations. For the origin band a lifetime of 1.21 ns was found by time-resolved photoionization, but the lifetime decreases quickly with excess energy and reaches around 30 ps at +800 cm^{-1}. Two deactivation channels were identified by coupled electron−nuclear dynamics simulations, internal conversion (IC) through a conical intersection to the S_0 electronic ground state, and intersystem crossing (ISC) to the almost degenerate T_4 ($n\pi^*$) state, which is allowed by the El-Sayed rules. Both processes will compete in the excited state deactivation. In order to access the conical intersection with S_0, an energy barrier has to be passed, which requires excess energy. This might explain the fairly sharp drop in lifetime with vibrational excitation in the S_1 state.

In cyclohexane solution only ISC occurring on a time scale of roughly 200 ps was experimentally found. The transient absorption spectrum recorded at long delay times resembles closely the computed absorption spectrum of the lowest triplet state. The deactivation within the triplet manifold is presumably rapid and cannot be time-resolved in the experiment. The lifetime of T_1 is long ($\tau_2 \geq 30$ ns) on the time scale of the experiment. Although cyclohexane is generally thought to have only a small impact on the potential energy surface of a molecule, it seems that the access to the conical intersection is hindered in solution. While IC and ISC compete in the gas phase, ISC dominates in cyclohexane.

For NTCDA we measured a lifetime of 16 ps at an excitation wavelength of 351 nm, which is close to the computed origin of the S_1 ($\pi\pi^*$) state. Again several triplet states are lower or equal in energy, and ISC to two of them is allowed by the El-Sayed rules.

In conclusion this work provides insight into the photophysics of NDCA, a molecule of importance in optoelectronics. Challenges for a correct description are the number of low-lying electronic states and the competition between IC and ISC. Both have been fully addressed. Employing a combination of surface-hopping simulations in the singlet states and electronic population dynamics in the full manifold of singlet and triplet states at a model level has allowed us to determine approximate branching ratios between internal conversion and intersystem crossing that are used to interpret the results of time-resolved experiments. For NTCDA, deactivation pathways similar to those found in NDCA are assumed.

ASSOCIATED CONTENT

Supporting Information

Photoionization mass spectra, static absorption spectra of NDCA and NTCDA, time-dependent populations of singlet and triplet states, and full references. This material is available free of charge via the Internet at http://pubs.acs.org.

AUTHOR INFORMATION

Corresponding Authors

*E-mail: ingo.fischer@uni-wuerzburg.de.
*E-mail: roland.mitric@uni-wuerzburg.de.

Notes

The authors declare no competing financial interest.

ACKNOWLEDGMENTS

This work was funded by the Deutsche Forschungsgemeinschaft within project FI 575/9-1 and the graduate research school GRK 1221. H.C.S. acknowledges financial support by the "Fonds der Chemischen Industrie". We thank Alex Schmiedl for recording the transient absorption spectra in solution.

REFERENCES

(1) Torsi, L.; Dodabalapur, A.; Cioffi, N.; Sabbatini, L.; Zambonin, P. G. NTCDA Organic Thin-Film-Transistor as Humidity Sensor: Weaknesses and Strengths. *Sens. Actuators, B* **2001**, *77*, 7−11.

(2) Falkenberg, C.; Uhrich, C.; Olthof, S.; Maennig, B.; Riede, M. K.; Leo, K. Efficient p-i-n Type Organic Solar Cells Incorporating 1,4,5,8-Naphthalenetetracarboxylic Dianhydride as Transparent Electron Transport Material. *J. Appl. Phys.* **2008**, *104*, 034506.

(3) Stadler, C.; Hansen, S.; Schöll, A.; Lee, T. L.; Zegenhagen, J.; Kumpf, C.; Umbach, E. Molecular Distortion of NTCDA upon Adsorption on Ag(111): A Normal Incidence X-Ray Standing Wave Study. *New J. Phys.* **2007**, *9*, 50.

(4) Bendounan, A.; Forster, F.; Schöll, A.; Batchelor, D.; Ziroff, J.; Umbach, E.; Reinert, F. Electronic Structure of 1 ML NTCDA/Ag(1 1 1) Studied by Photoemission Spectroscopy. *Surf. Sci.* **2007**, *601*, 4013−4017.

(5) Schöll, A.; Zou, Y.; Kilian, L.; Hübner, D.; Gador, D.; Jung, C.; Urquhart, S. G.; Schmidt, T.; Fink, R.; Umbach, E. Electron-Vibron Coupling in High-Resolution X-Ray Absorption Spectra of Organic Materials: NTCDA on Ag(111). *Phys. Rev. Lett.* **2004**, *93*, 146406.

(6) Schöll, A.; Zou, Y.; Schmidt, T.; Fink, R.; Umbach, E. High-Resolution Photoemission Study of Different NTCDA Monolayers on Ag(111): Bonding and Screening Influences on the Line Shapes. *J. Phys. Chem. B* **2004**, *108*, 14741−14748.

(7) Makowski, M.; Zazakowny, P.; Pawlikowski, M. T. The Resonance and Pre-Resonance Raman Scattering in the Low Energy 1 $^1B_{2u}$ and 1 $^1B_{3u}$ States of 1,4,5,8-Naphthalenetetracarboxy Dianhydride in Terms of DFT Methods. The Aggregation of NTCDA Molecules in the Ethanol and Methanol Solutions. *J. Raman Spectrosc.* **2013**, *44*, 1548−1556.

(8) Tachikawa, H.; Kawabata, H. Hybrid Density Functional Theory (DFT) Study on Electronic States of Halogen-Substituted Organic−

DOI: 10.1021/jp511843q
J. Phys. Chem. A XXXX, XXX, XXX−XXX

Inorganic Hybrid Compounds: Al-NTCDA. *Jpn. J. Appl. Phys.* **2005**, *44*, 3769−3773.
(9) Tachikawa, H.; Kawabata, H.; Ryoji Miyamoto, R.; Nakayama, K.; Yokoyama, M. Experimental and Theoretical Studies on the Organic−Inorganic Hybrid Compound: Aluminum-NTCDA Co-Deposited Film. *J. Phys. Chem. B* **2005**, *109*, 3139−3145.
(10) Fischer, K. H.; Fischer, I.; Bodi, A. Threshold Photoelectron Spectrum of Isolated NTCDA. *Z. Phys. Chem.* **2011**, *225*, 715−721.
(11) Sauther, J.; Wüsten, J.; Lach, S.; Ziegler, C. Gas Phase and Bulk Ultraviolet Photoemission Spectroscopy of 3,4,9,10-Perylene-Tetracarboxylic Dianhydride, 1,4,5,8-Naphthalene-Tetracarboxylic Dianhydride, and 1,8-Naphthalene-Dicarboxylic Anhydride. *J. Chem. Phys.* **2009**, *131*, 034711.
(12) Auerswald, J.; Engels, B.; Fischer, I.; Gerbich, T.; Herterich, J.; Krueger, A.; Lang, M.; Schmitt, H.-C.; Schon, C.; Walter, C. The Electronic Structure of Pyracene: A Spectroscopic and Computational Study. *Phys. Chem. Chem. Phys.* **2013**, *15*, 8151−8161.
(13) Herterich, J.; Gerbich, T.; Fischer, I. Excited-State Dynamics of the 2-Methylallyl Radical. *ChemPhysChem* **2013**, *14*, 3906−3908.
(14) Gerbich, T.; Herterich, J.; Köhler, J.; Fischer, I. Time-Domain Study of the S_3 State of 9-Fluorenone. *J. Phys. Chem. A* **2014**, *118*, 1397−1402.
(15) Barros, T. C.; Yunes, S.; Menegon, G.; Nome, F.; Chaimovich, H.; Politi, M. J.; Dias, L. G.; Cuccovia, I. M. Hydrolysis of 1,8- and 2,3-Naphthalic Anhydrides and the Mechanism of Cyclization of 1,8-Naphthalic Acid in Aqueous Solutions. *J. Chem. Soc., Perkin Trans. 2* **2001**, 2342−2350.
(16) Ghosh, S.; Biswas, S.; Mondal, M.; Basu, S. Photophysical Properties of 1,8-Naphthalic Anhydride in Aprotic Solvents: An Electron Acceptor in Excited State. *J. Lumin.* **2014**, *145*, 410−419.
(17) Stewart, W. W. Functional Connections between Cells as Revealed by Dye-Coupling with a Highly Fluorescent Naphthalimide Tracer. *Cell* **1978**, *14*, 741−759.
(18) Grabchev, I.; Moneva, I.; Bojinov, V.; Guittonneau, S. Synthesis and Properties of Fluorescent 1,8-Naphthalimide Dyes for Application in Liquid Crystal Displays. *J. Mater. Chem.* **2000**, *10*, 1291−1296.
(19) Kolosov, D.; Adamovich, V.; Djurovich, P.; Thompson, M. E.; Adachi, C. 1,8-Naphthalimides in Phosphorescent Organic LEDs: The Interplay between Dopant, Exciplex, and Host Emission. *J. Am. Chem. Soc.* **2002**, *124*, 9945−9954.
(20) Schon, C.; Roth, W.; Fischer, I.; Pfister, J.; Kaiser, C.; Fink, R. F.; Engels, B. Paracyclophanes as Model Compounds for Strongly Interacting π-Systems. Part 1. Pseudo-Ortho-Dihydroxy[2.2]-Paracyclophane. *Phys. Chem. Chem. Phys.* **2010**, *12*, 9339−9346.
(21) Kaiser, C.; Schmiedel, A.; Holzapfel, M.; Lambert, C. Long-Lived Singlet and Triplet Charge Separated States in Small Cyclophane-Bridged Triarylamine−Naphthalene Diimide Dyads. *J. Phys. Chem. C* **2012**, *116*, 15265−15280.
(22) Snellenburg, J. J.; Laptenok, S.; Seger, R.; Mullen, K. M.; Stokkum, I. H. M. v. Glotaran: A Java-Based Graphical User Interface for the R Package TIMP. *J. Stat. Software* **2012**, *49*, 1−22.
(23) Yanai, T.; Tew, D. P.; Handy, N. C. A New Hybrid Exchange-Correlation Functional Using the Coulomb-Attenuating Method (CAM-B3LYP). *Chem. Phys. Lett.* **2004**, *393*, 51−57.
(24) Weigend, F.; Ahlrichs, R. Balanced Basis Sets of Split Valence, Triple Zeta Valence and Quadruple Zeta Valence Quality for H to Rn: Design and Assessment of Accuracy. *Phys. Chem. Chem. Phys.* **2005**, *7*, 3297−3305.
(25) Santoro, F.; Improta, R.; Lami, A.; Bloino, J.; Barone, V. Effective Method to Compute Franck-Condon Integrals for Optical Spectra of Large Molecules in Solution. *J. Chem. Phys.* **2007**, *126*, 084509.
(26) Barone, V.; Bloino, J.; Biczysko, M.; Santoro, F. Fully Integrated Approach to Compute Vibrationally Resolved Optical Spectra: From Small Molecules to Macrosystems. *J. Chem. Theory Comput.* **2009**, *5*, 540−554.
(27) Tomasi, J.; Mennucci, B.; Cammi, R. Quantum Mechanical Continuum Solvation Models. *Chem. Rev.* **2005**, *105*, 2999−3094.
(28) Frisch, M. J.; Trucks, G. W.; Schlegel, H. B.; Scuseria, G. E.; Robb, M. A.; Cheeseman, J. R.; Scalmani, G.; Barone, V.; Mennucci, B.; Petersson, G. A.; et al. *Gaussian 09*, revision A.02; Gaussian Inc.: Wallingford, CT, 2009.
(29) Werner, H.-J.; Knowles, P. J.; Knizia, G.; Manby, F. R.; Schütz, M. *MOLPRO*, version 2012.1, a package of ab initio programs; Cardiff University: Cardiff, U.K., 2012.
(30) Berning, A.; Schweizer, M.; Werner, H.-J.; Knowles, P. J.; Palmieri, P. Spin-Orbit Matrix Elements for Internally Contracted Multireference Configuration Interaction Wavefunctions. *Mol. Phys.* **2000**, *98*, 1823−1833.
(31) Knowles, P. J.; Werner, H.-J. An Efficient Method for the Evaluation of Coupling Coefficients in Configuration Interaction Calculations. *Chem. Phys. Lett.* **1988**, *145*, 514−522.
(32) Knowles, P. J.; Werner, H.-J. Internally Contracted Multi-configuration-Reference Configuration Interaction Calculations for Excited States. *Theor. Chim. Acta.* **1992**, *84*, 95−103.
(33) Werner, H. J.; Knowles, P. J. An Efficient Internally Contracted Multiconfiguration−Reference Configuration Interaction Method. *J. Chem. Phys.* **1988**, *89*, 5803−5814.
(34) Knowles, P. J.; Werner, H.-J. An Efficient Second-Order MC SCF Method for Long Configuration Expansions. *Chem. Phys. Lett.* **1985**, *115*, 259−267.
(35) Werner, H. J.; Knowles, P. J. A Second Order Multi-configuration SCF Procedure with Optimum Convergence. *J. Chem. Phys.* **1985**, *82*, 5053−5063.
(36) Hehre, W. J.; Ditchfield, R.; Pople, J. A. Self-Consistent Molecular Orbital Methods. XII. Further Extensions of Gaussian-Type Basis Sets for Use in Molecular Orbital Studies of Organic Molecules. *J. Chem. Phys.* **1972**, *56*, 2257−2261.
(37) Tully, J. C. Molecular Dynamics with Electronic Transitions. *J. Chem. Phys.* **1990**, *93*, 1061−1071.
(38) Scholten, M., Semiempirische Verfahren mit Orthogonalisierungskorrekturen: Die OM3-Methode. Ph.D. Thesis, University of Düsseldorf, Germany, 2003.
(39) Koslowski, A.; Beck, M. E.; Thiel, W. Implementation of a General Multireference Configuration Interaction Procedure with Analytic Gradients in a Semiempirical Context Using the Graphical Unitary Group Approach. *J. Comput. Chem.* **2003**, *24*, 714−726.
(40) Patchkovskii, S.; Koslowski, A.; Thiel, W. Generic Implementation of Semi-Analytical CI Gradients for NDDO-Type Methods. *Theor. Chem. Acc.* **2005**, *114*, 84−89.
(41) Thiel, W. *MNDO Program*; Max-Planck-Intitut für Kohlenforschung: Mühlheim, Germany, 2007.
(42) Swope, W. C.; Andersen, H. C.; Berens, P. H.; Wilson, K. R. A Computer Simulation Method for the Calculation of Equilibrium Constants for the Formation of Physical Clusters of Molecules: Application to Small Water Clusters. *J. Chem. Phys.* **1982**, *76*, 637−649.
(43) Zazakowny, P.; Pawlikowski, M. T.; Sterzel, M. The Vibronic Structures of Absorption and Magnetic Circular Dichroism (MCD) in the Low Energy 1 $^1B_{2u}$ and 1 $^1B_{3u}$ States of 1,4,5,8-Naphthalenetetracarboxy Dianhydride. The Analysis in Terms of DFT and CASSCF Methods. *Chem. Phys. Lett.* **2009**, *472*, 55−59.
(44) El-Sayed, M. A. Triplet State. Its Radiative and Nonradiative Properties. *Acc. Chem. Res.* **1968**, *1*, 8−16.
(45) Siebrand, W. Mechanism of Radiationless Triplet Decay in Aromatic Hydrocarbons and the Magnitude of the Franck-Condon Factors. *J. Chem. Phys.* **1966**, *44*, 4055−4057.
(46) Englman, R.; Jortner, J. The Energy Gap Law for Radiationless Transitions in Large Molecules. *Mol. Phys.* **1970**, *18*, 145−164.
(47) Rosspeintner, A.; Lang, B.; Vauthey, E. Ultrafast Photochemistry in Liquids. *Annu. Rev. Phys. Chem.* **2013**, *64*, 247−271.
(48) Kollár, J.; Hrdlovič, P.; Chmela, S.; Sarakha, M.; Guyot, G. Synthesis and Transient Absorption Spectra of Derivatives of 1,8-Naphthalic Anhydrides and Naphthalimides Containing 2,2,6,6-Tetramethylpiperidine; Triplet Route of Deactivation. *J. Photochem. Photobiol., A* **2005**, *170*, 151−159.

DOI: 10.1021/jp511843q
J. Phys. Chem. A XXXX, XXX, XXX−XXX

(49) Spighi, G.; Gaveau, M.-A.; Mestdagh, J.-M.; Poisson, L.; Soep, B. Gas Phase Dynamics of Triplet Formation in Benzophenone. *Phys. Chem. Chem. Phys.* **2014**, *16*, 9610−9618.
(50) Zugazagoitia, J. S.; Almora-Díaz, C. X.; Peon, J. Ultrafast Intersystem Crossing in 1-Nitronaphthalene. An Experimental and Computational Study. *J. Phys. Chem. A* **2008**, *112*, 358−365.
(51) Mai, S.; Marquetand, P.; Richter, M.; González-Vázquez, J.; González, L. Singlet and Triplet Excited-State Dynamics Study of the Keto and Enol Tautomers of Cytosine. *ChemPhysChem* **2013**, *14*, 2920−2931.

DOI: 10.1021/jp511843q
J. Phys. Chem. A XXXX, XXX, XXX−XXX